Inverse Problems, Design and Optimization Symposium
Rio de Janeiro, Brazil, 2004

OPTIMIZATION OF HEATER SETTINGS TO PROVIDE SPATIALLY-UNIFORM TRANSIENT HEATING IN MANUFACTURING PROCESSES INVOLVING RADIANT HEATING

K. J. Daun and J. R. Howell
Department of Mechanical Engineering
The University of Texas at Austin
Austin, Texas, U. S. A.
jhowell@mail.utexas.edu

ABSTRACT

An optimization methodology is given for finding the heater settings that provide spatially-uniform transient heating in manufacturing processes involving radiant heating. Equations governing the transient temperature distribution and temperature sensitivity distribution over the product are derived using an infinitesimal-area technique, and solved numerically to calculate the objective function and gradient vector. Minimization is done using a quasi-Newton algorithm that incorporates an active set method to enforce design constraints. This methodology is demonstrated by finding the optimal transient heater settings of a two-dimensional annealing furnace.

INTRODUCTION

Radiant enclosures are found in diverse industrial settings. They are often used to uniformly heat a product according to a desired temperature history. Examples include annealing furnaces used in foundries, baking ovens used in food preparation, infrared heating systems that cure painted surfaces, and rapid thermal processing (RTP) chambers used to manufacture semiconductor wafers. In each case, the enclosure consists of a heater surface, several intermediate surfaces, and a design surface that contains the product to be processed. To design these systems, it is important to have an accurate model of the transient heater settings to size the heaters and other components of the enclosure. Having an accurate *a priori* estimate of the heater settings enables the use of high-gain controllers that quickly adjust the heaters to compensate for deviations from the desired temperature distribution over the design surface.

In the past, transient heater settings have been solved using a forward "trial-and-error" technique, in which the designer guesses the appropriate heater settings and then repeatedly evaluates and heuristically adjusts these settings until a satisfactory solution to the design problem is identified. Because of the complicated nature of the coupled heat transfer modes, an intuitive understanding of the system physics is elusive, so such design methodologies usually require many iterations, and the final solution is of limited quality.To overcome this difficulty, designers have adapted model-based control algorithms to design the transient heater settings. At any instant, the difference between the temperature measured at different locations on the design surface and the desired set-point temperature defines an error signal. This error signal is passed through a feedback loop to the controller, which adjusts the heater settings such to reduce the error signal. Model-based controllers were applied to design the heaters in RTP furnaces [1,2], and a furnace used in a continuous annealing process [3]. Despite the nonlinear nature of the problem, most model-based controllers use linear feedback algorithms that cannot accommodate the integrals in the radiosity equation that represent reflection and reradiation, so these effects are usually ignored; this induces large modeling errors into the controller, severely limiting theirn accuracy. Gwak and Masada [4] accounted for these effects by applying non-linear control laws coupled with embedded Tikhonov and TSVD regularization..

More recently, inverse design methodologies have been developed to solve this type of design problem. In this approach, both the desired temperature and the radiation heat input required to satisfy the sensible energy increase are specified over the design surface at different process times. The nonlinear system of equations is linearized and the resulting set of ill-conditioned linear equations is solved using regularization methods, starting from the first step. Each solution is used to define the right-

hand-side vector of the next time step. Multimiode radiant enclosure problems were solved by using TSVD regularization [5], and conjugate gradient regularization was used to find the transient heater settings that heated a design surface in a roll-through batch furnace according to a prescribed temperature history [6].

Unlike most model-based control algorithms, the inverse design approach can accommodate a sophisticated heat transfer model resulting in small modeling error. Nevertheless, a significant drawback of this method is that it is difficult to accommodate design constraints in the inverse design methodology, and because of this, solutions from regularization often include regions of negative heat flux over the heater surface. This condition cannot be realized in practical furnaces, so these regions are usually taken to be adiabatic, further impairing the solution quality.

Optimization through nonlinear programming overcomes many of these drawbacks. Here, an objective function, $F(\mathbf{\Phi})$, is defined in such a way that its minimum corresponds to the desired design outcome, which in this case is a temperature distribution over the design surface that both matches the desired temperature history and is also spatially uniform over the product throughout the process. The design parameters contained in $\mathbf{\Phi}$ define a set of functions that govern the heater output at any given time. Gradient-based minimization algorithms are then employed to find the set of design parameters, $\mathbf{\Phi}^*$, that minimize the objective function, so that $F(\mathbf{\Phi}^*) = Min[F(\mathbf{\Phi})]$. The design parameters contained in $\mathbf{\Phi}^*$ correspond to the transient heater settings that produce a temperature distribution over the design surface that most closely satisfies the design requirements.

Since the design parameters are modified in an intelligent way at each iteration based on the local objective function curvature, the optimization design methodology requires fewer iterations, and the solution quality is much better. This technique can also accommodate a more sophisticated system model than most control algorithms and consequently is less susceptible to modeling errors. Finally, unlike the inverse design methodology, the optimization methodology can easily accommodate design constraints. It is convenient to force the heat flux generated over the heater surface to lie within a specified operating range throughout the process.

Optimization techniques have been used on a limited basis to design industrial heating processes involving radiant enclosures. Unconstrained linear programming was used to obtain the optimal heater settings for a simplified linearized model of an RTP furnace [7], and to obtain an initial estimate of the heater settings so that a high-gain controller could be used to operate an RTP furnace[8]. Nonlinear programming was used to optimize the heater settings for a continuous roll-through industrial furnace operating at steady-state [9].

This paper presents an optimization technique that accounts for sensible energy storage in the enclosure walls as well as conjugate conduction and convection effects. The transient heater settings are optimized using a quasi-Newton minimization algorithm that incorporates an active set method to enforce the design constraints.

OPTIMIZATION STRATEGY

Figure 1 shows an example radiant enclosure. The design surface is located on the bottom surface and is irradiated by heaters on the top, which in turn are controlled throughout the process by the design parameters contained in $\mathbf{\Phi}$.

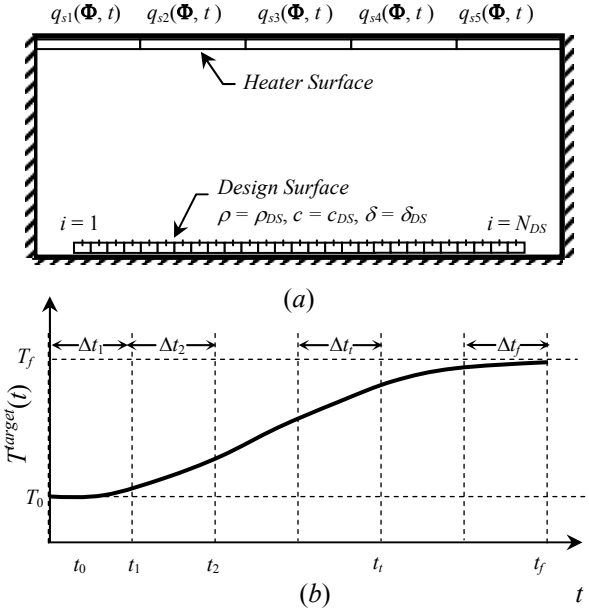

Fig. 1: Example of a transient radiant enclosure design problem: (*a*) radiant enclosure, and (*b*) desired set-point temperature history.

The design surface underside is insulated to prevent energy provided to the product by the heaters from leaving the system. As shown later,

solving this problem requires the discretization of both the temporal and spatial domains; the time domain is split into N_t time steps, the t^{th} time step having a duration Δt_t starting from time t_{t-1} and ending at t_t, and the design surface is split into N_{DS} discrete elements, with the i^{th} element having an area ΔA_i. Furthermore, it is assumed that the density, ρ_{DS}, thermal capacity, c_{DS}, and thickness, δ_{DS}, are uniform over the design surface.

The first step of this procedure is to define an objective function in such a way that it is minimized when (*a*) the average temperature over the design surface matches the desired set-point temperature at any instant, and (*b*) the temperature distribution over the design surface is uniform throughout the process. These design objectives could be satisfied individually by minimizing separate objective functions, each having a different minimum. Instead, these objective functions are combined to form a third objective function, whose minimum represents a trade-off between the two design objectives.

The first design objective is satisfied by minimizing the difference between the sensible energy provided to the design surface by the heaters, and the energy required to heat the design surface to the set-point temperature. The heater settings that accomplish this goal at every time step are found by minimizing

$$F_1(\mathbf{\Phi}) = \gamma_2 \sum_{t=1}^{N_t} \left\{ \left[Q_{t-1\to t}^{added}(\mathbf{\Phi}) - Q_{t-1\to t}^{target} \right]^2 + (1-\gamma_2)\left[Q_{0-tf}^{deficit}(\mathbf{\Phi}) \right]^2 \right\}, \quad (1)$$

where $Q_{t-1\to t}^{added}(\mathbf{\Phi}) - Q_{t-1\to t}^{target}(\mathbf{\Phi})$ is the difference between the sensible energy increase in the design surface provided by the heaters during the t^{th} time step and the sensible energy that must be added to achieve the desired temperature increase over the t^{th} time step,

$$Q_{t-1\to t}^{added}(\mathbf{\Phi}) - Q_{t-1\to t}^{target} = \rho_{DS} c_{DS} \delta_{DS} \times \left\{ \sum_{i=1}^{N_{DS}} \left[T_i(\mathbf{\Phi}, t_t) - T_i(\mathbf{\Phi}, t_{t-1}) \right] \Delta A_i - \left[T^{target}(t_t) - T^{target}(t_{t-1}) \right] A_{DS} \right\}, \quad (2)$$

and $Q_{0\to tf}^{deficit}(\mathbf{\Phi})$ is the difference between the sensible energy added to the design surface throughout the process and that which must be added to obtain the set point temperature at the end of the process,

$$Q_{0\to tf}^{deficit}(\mathbf{\Phi}) = \rho_{DS} c_{DS} \delta_{DS} \times \sum_{i=1}^{N_{DS}} \left[T_i(\mathbf{\Phi}, t_f) - T^{target}(t_f) \right] \Delta A_i \,. \quad (3)$$

These quantities are shown schematically in Fig. 2. Minimizing the first part of $F_1(\mathbf{\Phi})$ produces an average design surface temperature profile that best matches the slope of the set-point temperature. There is likely to be a small difference between $Q_{t-1\to t}^{added}(\mathbf{\Phi}^*)$ and $Q_{t-1\to t}^{target}$ at every time step, which may accumulate over the process duration. The second term in $F_1(\mathbf{\Phi})$ ensures that this error is sufficiently small. The heuristic parameter γ_2 is adjusted by the designer to achieve an average design surface temperature that closely matches the desired set-point temperature throughout the process.

The second design objective is to maintain a uniform temperature distribution over the design surface throughout the process. The heater settings that satisfy this condition are found by minimizing the variance between the temperature values calculated at discrete locations over the design surfaces, averaged over all time steps,

$$F_2(\mathbf{\Phi}) = \frac{1}{N_t N_{DS}} \sum_{t=1}^{N_t} \sum_{i=1}^{N_{DS}} \left[T_i(\mathbf{\Phi}, t_t) - \overline{T}(\mathbf{\Phi}, t_t) \right]^2 \quad (4)$$

As previously mentioned, the objective functions defined in Eqs. (1) and (4) pertain to different design objectives, and both of these functions are minimized by different sets of $\mathbf{\Phi}$, i.e. $\mathbf{\Phi}_1^* \neq \mathbf{\Phi}_2^*$.

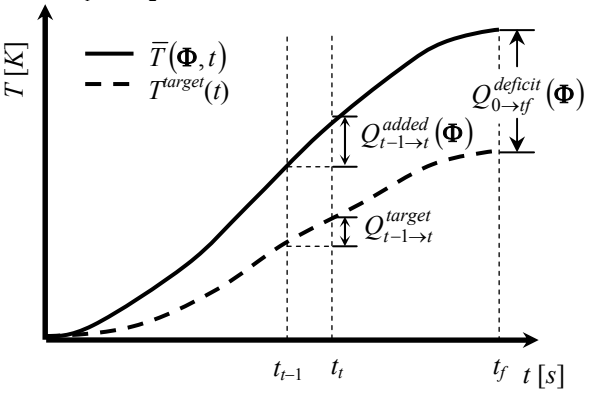

Fig. 2: Relationship between $Q_{t-1\to t}^{added}(\mathbf{\Phi})$, $Q_{t-1\to t}^{target}$, $Q_{0\to tf}^{deficit}(\mathbf{\Phi})$, and design surface temperature.

A hybrid objective function is formed by combining these two objective functions,

$$F(\mathbf{\Phi}) = C\left[\gamma_1 F_1(\mathbf{\Phi}) + (1-\gamma_1) F_2(\mathbf{\Phi})\right], \quad (5)$$

where γ_1 is chosen based on the relative importance of the two design objectives in a particular application, and C is a scaling parameter. The set of design parameters $\boldsymbol{\Phi}^*$ that minimizes Eq. (5) is a compromise between a solution where the average design surface temperature closely follows the set-point temperature and one having a near-uniform temperature distribution over the design surface throughout the process.

Since $F(\boldsymbol{\Phi})$ is continuously differentiable, $\boldsymbol{\Phi}^*$ is found iteratively using gradient-based minimization. At the k^{th} iteration, the design parameters are updated by first choosing a search direction, $\boldsymbol{p}^k$, based on the objective function topography. Next, a step size, α^k, is chosen, often by minimizing $F(\boldsymbol{\Phi}^k+\alpha^k\boldsymbol{p}^k)$. Providing that the constraints are not violated, the design parameters are then updated by taking a "step" in the $\boldsymbol{p}^k$ direction, $\boldsymbol{\Phi}^{k+1} = \boldsymbol{\Phi}^k + \alpha^k\boldsymbol{p}^k$.

Newton's method usually requires the fewest iterations to minimize the objective function; at each iteration, $\boldsymbol{p}^k$ is found by solving

$$\nabla^2 F\left(\boldsymbol{\Phi}^k\right)\boldsymbol{p}^k = -\nabla F\left(\boldsymbol{\Phi}^k\right). \tag{6}$$

If the second-order design sensitivities contained in $\nabla^2 F(\boldsymbol{\Phi})$ are expensive to calculate, the quasi-Newton method is often more suitable. In this scheme, the search direction is given by

$$\mathbf{B}^k\ \boldsymbol{p}^k = -\nabla F\left(\boldsymbol{\Phi}^k\right), \tag{7}$$

where $\mathbf{B}^k$ approximates $\nabla^2 F(\boldsymbol{\Phi})$. Initially, $\mathbf{B}^0$ is equal to the identity matrix and $\boldsymbol{p}^0$ is the steepest-descent direction. In subsequent iterations, the Hessian approximation is updated and improved using values of $F(\boldsymbol{\Phi})$ and $\nabla F(\boldsymbol{\Phi})$ from previous iterations. The most popular way of doing this is with the Broyden-Fletcher-Goldfarb-Shanno (BFGS) update,

$$\mathbf{B}^{k+1} = \mathbf{B}^k - \frac{\mathbf{B}^k \boldsymbol{s}^k \boldsymbol{s}^{k\,T} \mathbf{B}^k}{\boldsymbol{s}^{k\,T} \mathbf{B}^k \boldsymbol{s}^k} + \frac{\boldsymbol{y}^k \boldsymbol{y}^{k\,T}}{\boldsymbol{y}^{k\,T} \boldsymbol{p}^k}, \tag{8}$$

with $\mathbf{s}^k = \boldsymbol{\Phi}^{k+1} - \boldsymbol{\Phi}^k$ and $\boldsymbol{y}^k = \nabla F(\boldsymbol{\Phi}^{k+1}) - \nabla F(\boldsymbol{\Phi}^{k+1})$.

Since $\mathbf{B}^k$ approximates $\nabla^2 F(\boldsymbol{\Phi})$ accurately only after several iterations, the quasi-Newton method requires more iterations than Newton's method to find $\boldsymbol{\Phi}^*$. Nevertheless, the quasi-Newton method is usually more computationally efficient in cases where the second-order objective sensitivities are expensive to calculate.

In order to find $\boldsymbol{p}^k$, it is necessary to evaluate $F(\boldsymbol{\Phi})$ and $\nabla^2 F(\boldsymbol{\Phi})$, which in turn are calculated using temperatures, $T_i(\boldsymbol{\Phi},t_t)$, and first-order temperature sensitivities, $\partial T_i(\boldsymbol{\Phi},t_t)/\partial\Phi_p$, at discrete locations over the design surface throughout the process. A technique for doing this is presented in the next section.

CALCULATION OF TEMPERATURE AND TEMPERATURE SENSITIVITES

An infinitesimal-area analysis [10] is used to derive the equations governing the temperature and temperature sensitivities. The first step of the analysis is to identify a suitable parametric representation for the enclosure. The enclosure geometry is specified by

$$\boldsymbol{r} = \boldsymbol{C}(u) = \{P(u), Q(u)\}^T,\ a \le u \le b, \tag{9}$$

where the position vector $\boldsymbol{r}$ carves out the enclosure cross section in the x–y plane as u varies over its domain.

Once the geometry is parameterized, either the temperature, $T(u,\boldsymbol{\Phi},t)$, or the heat flux, $q_s(u,\boldsymbol{\Phi},t)$, is specified at every location on the enclosure surface at any time t. In particular, the transient heat flux distribution over the heater surfaces is specified as a function of the heater settings contained in $\boldsymbol{\Phi}$ and the adiabatic boundary condition is enforced over the design surface throughout the process. The thermal properties $\varepsilon(u)$, $\kappa(u)$, $\rho(u)$, $c(u)$, and the wall thickness, $\delta(u)$, are also specified parametrically.

Once the enclosure has been represented parametrically, the equation relating the radiosity distribution, $q_o(u,\boldsymbol{\Phi},t)$, to the temperature distribution, $T(u, \boldsymbol{\Phi}, t)$, is derived by performing an energy balance on an infinitely long wall element having a thickness $\delta(u)$ and an infinitesimal chord length $J(u)du$, as shown in Fig. 3, where the surface discriminant, $J(u)$, is given by

$$J(u) = \left\{\left[\frac{\partial P(u)}{\partial u}\right]^2 + \left[\frac{\partial Q(u)}{\partial u}\right]^2\right\}^{1/2}, \tag{10}$$

In addition to radiation heat transfer, three other modes of heat transfer enter or leave the wall element: $q_{cond}(u,\boldsymbol{\Phi},t)$ is the net rate of heat transfer entering the wall element by conduction from the surrounding enclosure wall,

$$q_{cond}(u,\boldsymbol{\Phi},t) = \frac{1}{J(u)}\frac{\partial}{\partial u}\left[\frac{\kappa(u)}{J(u)}\frac{\partial T(u,\boldsymbol{\Phi},t)}{\partial u}\right], \tag{11}$$

$q_{conv}(u, \boldsymbol{\Phi}, t)$ is the rate of convection transferred from the wall element to the fluid contained within the enclosure,

$$q_{conv}(u, \boldsymbol{\Phi}, t) = h(u,t)\left[T(u, \boldsymbol{\Phi}, t) - T_\infty(t)\right], \tag{12}$$

and $q_s(u, \boldsymbol{\Phi}, t)$ is the rate that any other type of heat transfer enters the wall element by non-radiative means. All of these terms are per unit

internal area of the infinitesimal wall element. (Convection heat transfer with the fluid surrounding the enclosure has been excluded to simplify the heat transfer model.)

Setting the net rate of conduction, convection, and thermal radiation heat transfer entering the infinitesimal wall element equal to the rate of sensible energy storage, we find

$$\sigma T^4(u,\boldsymbol{\Phi},t)-\int_a^b \sigma T^4(u',\boldsymbol{\Phi},t)\,k(u,u')\,du' = \frac{b(u,\boldsymbol{\Phi},t)}{\varepsilon(u)}-\int_a^b \frac{1-\varepsilon(u')}{\varepsilon(u')}\,b(u',\boldsymbol{\Phi},t)\,k(u,u')\,du', \tag{13}$$

where $k(u, u')$ contains geometric terms derived from Eq. (9), and $b(u, \boldsymbol{\Phi}, t)$ represents the difference between the net non-radiative heat transfer into an infinitesimal wall element and the sensible energy stored within that element,

$$b(u,\boldsymbol{\Phi},t)=q_s(u,\boldsymbol{\Phi},t)+q_{cond}(u,\boldsymbol{\Phi},t) - q_{conv}(u,\boldsymbol{\Phi},t)-\rho(u)c(u)\delta(u)\frac{\partial T(u,\boldsymbol{\Phi},t)}{\partial t} \tag{14}$$

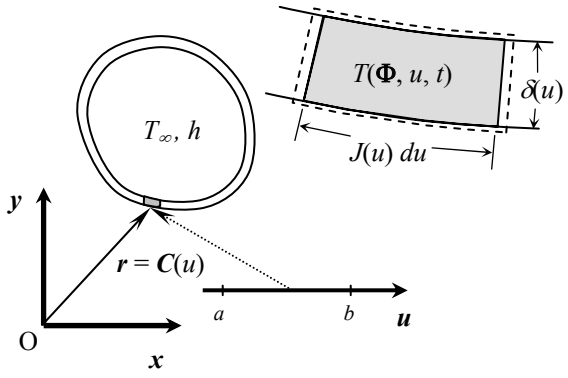

Fig. 3: Parametric representation of the radiant enclosure, and infinitesimal wall element used to form governing temperature equation.

The equations governing the temperature sensitivity are found by differentiating Eqs. (13) and (14) with respect to the design parameter of interest. By applying Liebnitz's rule to Eq. (13) and noting that the integral bounds are independent of u, the temperature sensitivities are

$$4\sigma T^3(u,\boldsymbol{\Phi},t)\frac{\partial T(u,\boldsymbol{\Phi},t)}{\partial \Phi_p} - \int_a^b 4\sigma T^3(u',\boldsymbol{\Phi},t)\frac{\partial T(u',\boldsymbol{\Phi},t)}{\partial \Phi_p}\,k(u,u')\,du' = \frac{1}{\varepsilon(u)}\frac{\partial b(u,\boldsymbol{\Phi},t)}{\partial \Phi_p}-\int_a^b \frac{1-\varepsilon(u')}{\varepsilon(u')}\frac{\partial b(u',\boldsymbol{\Phi},t)}{\partial \Phi_p}\,k(u,u')\,du', \tag{15}$$

where

$$\frac{\partial b(u,\boldsymbol{\Phi},t)}{\partial \Phi_p}=\frac{\partial q_s(u,\boldsymbol{\Phi},t)}{\partial \Phi_p}-h(u,t)\frac{\partial T(u,\boldsymbol{\Phi},t)}{\partial \Phi_p} + \frac{1}{J(u)}\frac{\partial}{\partial u}\left[\frac{\kappa(u)}{J(u)}\frac{\partial^2 T(u,\boldsymbol{\Phi},t)}{\partial u\,\partial \Phi_p}\right] - \rho(u)c(u)\delta(u)\frac{\partial^2 T(u,\boldsymbol{\Phi},t)}{\partial t\,\partial \Phi_p}. \tag{16}$$

Since analytical solutions to integro-differential equations are usually not tractable, the temperature and temperature sensitivity distributions must be solved numerically. The parametric domain is divided into N elements, with the i^{th} element centered on u_i and having a width Δu_i. Each of the elements in parametric space corresponds to an infinitely long wall element having a finite thickness, as shown in Fig. 4. The time domain is discretized into N_t time steps starting from t_0 to $t_{Nt} = t_f$ in intervals of Δt_t.

The integrals in Eqs (13) and (15) are approximated as discrete summations,

$$\int_a^b x(u)\,k(u,u')\,du' \approx \sum_{j=1}^{N} x(u_j)\,dF_{i-stripj}, \tag{17}$$

where $x(u)$ is the integrated quantity and $dF_{i-stripj}$ is the configuration factor between a point on the enclosure at u_i and the exposed surface of a finite wall element centered at u_j. The spatial temperature derivatives in Eq. (14) are rewritten using a second-order central difference approximation, and the temporal derivatives are approximated using a first-order backwards difference operator.

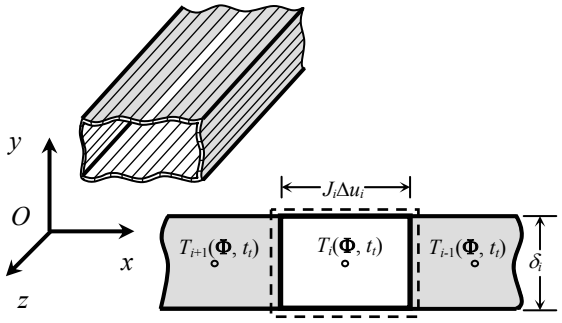

Fig. 4: Discretization of the radiant enclosure into finite wall elements.

The integro-differential equations governing the temperature can be rewritten in discrete form,

$$\hat{T}_i^4(\boldsymbol{\Phi},\tau_t) - \sum_{\substack{j=1\\ j\neq i}}^{N} \hat{T}_j^4(\boldsymbol{\Phi},\tau_t)\, dF_{i-stripj} = \frac{\hat{b}_i(\boldsymbol{\Phi},\tau_t,\tau_{t-1})}{\varepsilon_i} - \sum_{\substack{j=1\\ j\neq i}}^{N} \left[\frac{1-\varepsilon_j}{\varepsilon_j}\right] \hat{b}_i(\boldsymbol{\Phi},\tau_t,\tau_{t-1})\, dF_{i-stripj}, \quad (18)$$

where $\varepsilon_i = \varepsilon(u_i)$, and the time and temperature terms are represented non-dimensionally by $\tau_t = (t_t - t_0)/(t_f - t_0)$, and $\hat{T}_i(\boldsymbol{\Phi},\tau_t) = T(u_i,\boldsymbol{\Phi},t)/T_s$, where T_s is a scaling temperature. Also,

$$\begin{aligned}\hat{b}_i(\boldsymbol{\Phi},\tau_t,\tau_{t-1}) &= \hat{q}_{si}(\boldsymbol{\Phi},\tau_t) \\ &+ C_{cond}\,\frac{\hat{\kappa}_i}{\hat{J}_i^2}\left[\frac{\hat{T}_{i+1}(\boldsymbol{\Phi},\tau_t) - 2\hat{T}_i(\boldsymbol{\Phi},\tau_t) + \hat{T}_{i-1}(\boldsymbol{\Phi},\tau_t)}{2\Delta u_i}\right] \\ &- C_{conv}\,\hat{h}_i(\tau_t)\left[\hat{T}_i(\boldsymbol{\Phi},\tau_t) - \hat{T}_\infty\right] \\ &+ C_{trans}\,\hat{\rho}_i\hat{c}_i\hat{\delta}_i\,\frac{\hat{T}_i(\boldsymbol{\Phi},\tau_t) - \hat{T}_i(\boldsymbol{\Phi},\tau_{t-1})}{\Delta\tau_t},\end{aligned} \quad (19)$$

where $\hat{q}_{si}(\boldsymbol{\Phi},\ \tau_t) = q_s(u_i,\ \boldsymbol{\Phi},\ t_t)/T_s$ and $\hat{h}(\tau_t) = h(u_i,\ t_t)/\overline{h}$. The enclosure properties are represented by $\hat{\kappa}_i = \kappa(u_i)/\kappa_s$, $\hat{\rho}_i = \rho(u_i)/\rho_s$, $\hat{c}_i = c(u_i)/c_s$, $\hat{\delta}_i = \delta(u_i)/\delta_s$, and $\hat{J}_i = J(u_i)/L_c$, where L_c is a characteristic length. The coefficients C_{cond}, C_{conv}, and C_{trans} are

$$C_{cond} = \frac{\kappa_s}{\sigma T_s^3 L_c^2}, \quad (20)$$

$$C_{conv} = \frac{\overline{h}}{\sigma T_s^3}, \quad (21)$$

and

$$C_{trans} = \frac{\rho_s c_s \delta_s}{\sigma T_s^3 (t_f - t_0)}, \quad (22)$$

and their magnitudes indicate the importance of conduction, convection and sensitive energy storage relative to radiation.

Writing Eqs. (18) and (19) for every wall element results in a matrix equation governing the temperature of the enclosure surfaces at time τ_t,

$$\mathbf{A}_1\boldsymbol{x}_1(\boldsymbol{\Phi},\tau_t) + \mathbf{A}_2\boldsymbol{x}_2(\boldsymbol{\Phi},\tau_t) = \boldsymbol{c}(\boldsymbol{\Phi},\tau_t,\tau_{t-1}), \quad (23)$$

where $x_{1,i}(\boldsymbol{\Phi},\tau_t) = \hat{T}_i^4(\boldsymbol{\Phi},\tau_t)$ and $x_{2,i}(\boldsymbol{\Phi},\tau_t) = \hat{T}_i(\boldsymbol{\Phi},\tau_t)$. In order to solve for the transient temperature distribution, Eq. (23) must be linearized to form a related matrix equation,

$$\mathbf{A}(\boldsymbol{\Phi},\tau_{t-1})\,\boldsymbol{x}(\boldsymbol{\Phi},\tau_t) = \boldsymbol{b}(\boldsymbol{\Phi},\tau_t,\tau_{t-1}), \quad (24)$$

where $x_i(\boldsymbol{\Phi},\tau_t) = \hat{T}_i^4(\boldsymbol{\Phi},\tau_t)$ or $\hat{T}_i(\boldsymbol{\Phi},\tau_t)$, depending on which linearization scheme is used. The transient temperature distribution is then solved by first guessing a solution at $\tau = 0$ and then writing and solving Eq. (24) at each time step using the temperature distribution from the previous time step to form the **A** matrix and ***b*** vector. Not all linearization schemes will result in a convergent solution for a given problem [11], so the method used to linearize Eq. (23) must be chosen based on the relative magnitudes of the coefficients defined in Eqs. (20)–(22).

Following a similar procedure for Eqs. (15) and (16) results in another matrix equation governing the temperature sensitivities,

$$\mathbf{dA}(\boldsymbol{\Phi},\tau_{t-1})\,\boldsymbol{x}'(\boldsymbol{\Phi},\tau_t) = \boldsymbol{b}'(\boldsymbol{\Phi},\tau_t,\tau_{t-1}), \quad (25)$$

where $x_i'(\boldsymbol{\Phi},\tau_t) = \partial\hat{T}_i(\boldsymbol{\Phi},\tau_t)/\partial\boldsymbol{\Phi}_p$. Assuming the temperature distribution has been solved for, the sensitivities are found by guessing a sensitivity distribution at t_0 and then writing and solving Eq. (25) at each time step using the sensitivities from the previous distribution.

IMPLEMENTATION

The design methodology described in the previous section is demonstrated by using it to optimize the heater settings of a two-dimensional annealing furnace (Fig. 5). The top surface has ten uniformly-spaced heaters, the two side walls are refractory surfaces, and the design surface is on the bottom of the enclosure. The heater and refractory surfaces are assumed to have the properties of refractory brick, and the design surface is a slab of AISI 1010 steel. All enclosure surfaces are assumed to be gray and diffuse, and their properties are summarized in Table 1.

The objective is to uniformly heat the steel at a linear ramp rate from 300 *K* to 500 *K* over a five-hour period. It is assumed that the enclosure surfaces are initially at 300 *K*, at which point the heaters are activated and the surfaces are exposed to a fluid at T_∞ = 500 *K* and h = 5 W/m^2K. The enclosure surfaces are assumed to be thermally isolated from each other, which is enforced by insulating the surface edges.

Because of symmetry, the heaters are controlled in pairs and are numbered as shown in Fig. 5. In particular, if u_i lies on the h^{th} heater,

$$\begin{aligned}\hat{q}_{si}(\boldsymbol{\Phi},\tau) = {} & \Phi_{4h}(1-\tau)^3 + \Phi_{4h+1}3(1-\tau)^2\tau \\ & + \Phi_{4h+1}3(1-\tau)\tau^2 + +\Phi_{4h+1}\tau^3,\end{aligned} \quad (26)$$

where $\{\Phi_{4h}, \Phi_{4h+1}, \Phi_{4h+2}, \Phi_{4h+3}\}^T$ is a subspace of $\boldsymbol{\Phi}$; thus, 20 design parameters specify the heat flux distribution over the heater surface throughout the process. Controlling the heater output in this way reduces the dimension of the minimization problem. Because the basis functions in Eq. (26) sum to unity for any value of τ, the heater outputs can be constrained to lie between upper and lower bounds by applying the same bounds to the corresponding design parameters. The heat flux is constrained to lie between $0 \le \hat{q}_{s\,h}(\boldsymbol{\Phi}, \tau) \le 10$ by incorporating an active set method [12] into the BFGS minimization routine.

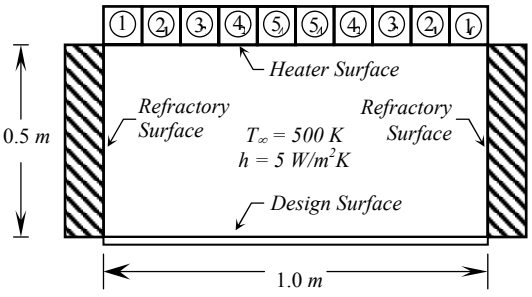

Fig. 5: Example design problem. (Heater numbers are shown in circles.)

Table 1: Enclosure surface properties.

	Heater Surface	Refractory Surface	Design Surface
κ [W/m K]	1.0	1.0	63.9
ρ [kg/m^3]	2645	2645	7832
c [J/kg K]	960	960	487
δ [m]	0.1	0.1	0.02
ε	0.8	0.8	0.4

The problem is non-dimensionalized using $L_c = 1m$, $\bar{h} = 5$ W/m^{2}K, and $T_s = 1000$ K, while κ_s, ρ_s, c_s, and δ_s, are set equal to the design surface properties. Substituting these values into Eqs. (20)–(22) results in $C_{cond} = 1.1270$, $C_{conv} = 0.082$, and $C_{trans} = 0.0747$.

The magnitudes of the non-dimensional coefficients indicate that conduction effects dominate the model, so Eq. (18) is linearized by lagging the emissive power terms. This results in a matrix equation of the form of Eq. (24), where $\mathbf{A}$ contains the conduction, convection, and sensible energy storage temperature coefficients, $\boldsymbol{b}(\boldsymbol{\Phi}, \tau_t, \tau_{t-1})$ is composed of heat fluxes from the current time step and terms from the conduction boundary condition, fluid temperature, sensible energy, and thermal radiation from the previous time step, and $x_i(\boldsymbol{\Phi}, \tau_t) = \hat{T}_i(\boldsymbol{\Phi}, \tau_t)$. Solving for the sensitivities results in

$$\boldsymbol{A}\,\boldsymbol{x}'\left(\boldsymbol{\Phi}, \tau_t\right) = \boldsymbol{b}'\left(\Phi, \tau_t, \tau_{t-1}\right), \qquad (27)$$

where $\boldsymbol{b}'(\boldsymbol{\Phi}, \tau_t, \tau_{t-1})$ contains the heat flux, sensible energy, and thermal radiation sensitivities with respect to Φ_p, and $\boldsymbol{x}'_i(\boldsymbol{\Phi}, \tau_t) = \partial \hat{T}_i(\boldsymbol{\Phi}, \tau_t)/\partial \boldsymbol{\Phi}_p$. Thus, $\mathbf{A}$ needs to be formed and inverted only once at each time step to calculate both the temperature distribution and sensitivities.

The optimal heater settings are found by minimizing the objective function in Eq. (5). The parametric and time domains were discretized using $N = 240$ wall elements and $N_t = 500$ time steps to calculate $F(\boldsymbol{\Phi})$ and $\nabla F(\boldsymbol{\Phi})$ throughout the optimization process. The minimization was carried out starting from $\boldsymbol{\Phi}_i^0 = 1$, $i = 1 \ldots 20$, and was stopped when $\|\nabla F_{FR}(\boldsymbol{\Phi})\| \le 10^{-6}$, where $\nabla F_{FR}(\boldsymbol{\Phi})$ contains the first-order sensitivities with respect to the unconstrained design parameters. A good result was obtained with $C = 100$, $\gamma_1 = 0.99$, and $\gamma_2 = 0.995$.

A local minimum of $F(\boldsymbol{\Phi}^*) = 2.284 \times 10^{-3}$ was found after 30 iterations. The optimal heater settings are shown in Fig. 6, while the resulting transient temperature response of the design surface is in Fig. 7. The maximum deviation of the average temperature from the set-point temperature was 7.15% at the end of the process. A better solution might be found by using higher-order splines to control the heaters, but the thermal inertia of the design surface severely limits the response sensitivity of the design surface. A near uniform temperature distribution is maintained throughout the process; the maximum standard deviation from the average design surface temperature is 0.006%, occurring at $\tau = 1$.

Refinement studies verified that a sufficient number of wall elements and time steps were used to ensure grid-independence.

CONCLUSIONS

An optimization method is given for finding optimal heater settings in radiant enclosures used in manufacturing processing applications. The method works by defining an objective function

that is minimized when the design surface temperature matches the set-point temperature, and the temperature distribution is uniform over the design surface throughout the process. Once this is done, the heater settings are optimized by minimizing the objective function iteratively through the BFGS method incorporating an active set method to enforce design constraints.

Because the design is improved systematically at each iteration, this technique requires far less design time and provides a much better final solution than the traditional "trial-and-error" approach, which relies on the designer's intuition and experience. This method can also accommodate a sophisticated heat transfer model and design constraints that help ensure that the optimal industrial solution can be implemented.

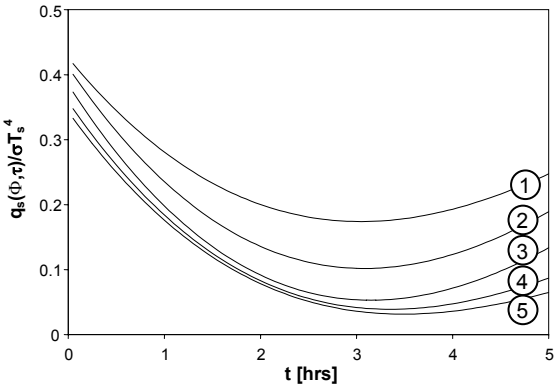

Fig. 6: Optional heater settings.

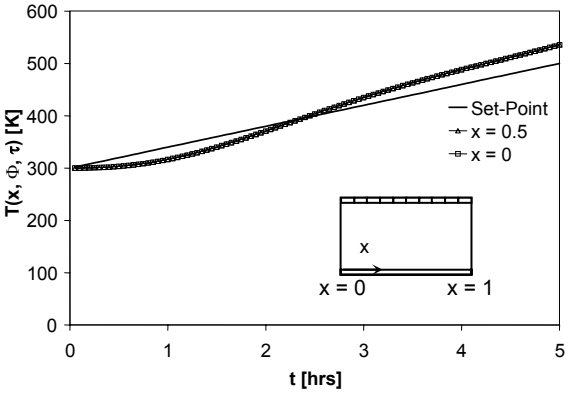

Fig. 7: Optimal design surface temperature.

ACKNOWLEGEMENTS

This work was supported by National Science Foundation grants CTS 70545, DMI 9072217, and DMI 0217927.

REFERENCES

1. Breedjik, T. Edgar, T. F., and Trachtenberg, I., Model-based control of rapid thermal processes, *Proc. American Control Conf.*, Baltimore, MD. (1994)

2. BalakrishnanK. S., and Edgar, T. F., Model-based control in rapid thermal processing, *Thin Solid Films*, **365**, p. 322 (2000)

3. Yoshitani, N., and Hasegawa, A., Model-based control of strip temperature for the heating furnace in continuous annealing, *IEEE Trans. on Control Systems*, **6**, 2, p. 146 (1998)

4. Gwak, K. W., and Masada, G., Structural analysis of nonlinear control systems using singular value decomposition, *Proc. 2000 IMECE*, New York, NY (2000)

5. Franca, F. H. R., Howell, J. R., Ezekoye, O. A., and Morales, J. C., Inverse design of thermal systems*, Advances in Heat Transfer, J. P. Hartnett and T. F. Irvine, Eds.*, 36, Academic Press (2002)

6. Ertürk, H., Ezekoye, O. A., and Howell, J. R., The application of an inverse formulation in the design of boundary conditions for transient radiating enclosures, *J. Heat Trans.*, **124**, 6 (2002)

7. Norman, S. A., Optimization of transient temperature uniformity in RTP systems, *IEEE Trans. on Electron Devices*, **39**, 1 (1992)

8. Cho, Y. M., Gyugyi, P., Control of rapid thermal processing: a system theoretic approach, *IEEE Trans. on Control Sys. Tech.*, **5**, 6, (1997)

9. Fedorov, A. G., Lee, K. H., and Viskanta, R., Inverse optimal design of the radiant heating in materials processing and manufacturing, *J. Materials Eng. and Performance*, **7**, 6 (1998)

10. Daun, K. J., and Hollands, K. G. T., Infinitesimal radiative analysis using parametric surface representation, through NURBS, *J. Heat Trans*, **123**, 2 (2001)

11. Siegel, R., and Howell, J. R., *Thermal Radiation Heat Transfer, 4th Ed.*, Taylor and Francis, New York, NY, p. 385 (2002)

12. Gill, P. E., Murray, W., and Wright, M. H., *Practical Optimization*, Academic Press, San Diego, CA, p. 167 (1986)